THE JOURNAL OF PHYSICAL CHEMISTRY C

Article

pubs.acs.org/JPCC

Reaction Kinetics and Formation Mechanism of TiO_2 Nanorods in Solution: An Insight into Oriented Attachment

Cheng-Si Tsao,*[,†] Chih-Min Chuang,[†] Chun-Yu Chen,[‡] Yu-Ching Huang,[†] Hou-Chin Cha,[†] Fan-Hsuan Hsu,[†] Charn-Ying Chen,[†] Yu-Chieh Tu,[§] and Wei-Fang Su*[,§]

[†]Institute of Nuclear Energy Research, Longtan, Taoyuan 32546, Taiwan ROC

[‡]National Synchrotron Radiation Research Center, Hsinchu 30077, Taiwan ROC

[§]Department of Materials Science and Engineering, National Taiwan University, Taipei 10617, Taiwan ROC

Supporting Information

ABSTRACT: The reaction kinetics and formation mechanism of oriented attachment for shaped nanoparticles in solution are not well-understood. We present the reaction kinetics and formation mechanism of organic-capped anatase TiO_2 nanorods in solution as a case study for the oriented attachment process using small-angle X-ray scattering (SAXS) and transmission electronic microscopy. The SAXS analysis qualitatively and quantitatively provides in-depth understanding of the mechanism, including the structural evolution, interparticle interaction, and spatial orientation of nanoparticles developed from nanodots to nanorods during the nucleation, isotropic, and anisotropic growth steps. The present study demonstrates the growth details of oriented attachment of nanoparticles in solution. An ordered lamellar structure in the solution is constructed by the balance of interaction forces among surface ligands, functional groups, and solvent molecules serving as a natural template. The template allows the alignment of spherical nanoparticles into ordered chain arrays and facilitates simultaneous transformation from spherical to rod shape via proximity attachment. The proposed model reveals an insight into the oriented attachment mechanism. This multistep formation mechanism of TiO_2 nanorods in solution can provide the fundamental understanding of how to tune the shape of nanoparticles and further control the aggregation of spatial nanorod networks in solution.

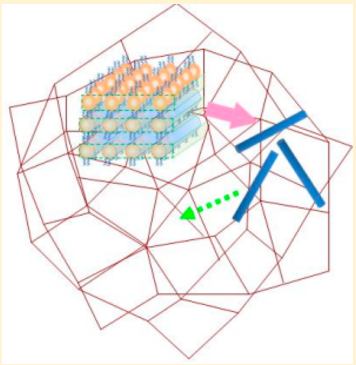

INTRODUCTION

Inorganic nanoparticles play important roles in various fields of science and applications. Especially, one-dimensional nanostructures (rods and wires) exhibit unique electrical and optical properties that depend on the size, shape, and interparticle reaction.[1−5] It is essential to control the size, shape, interaction, and growth of nanoparticles for exploring the nanostructure−property relationship. Investigating the reaction kinetics and formation mechanism of anisotropic particles would be the key for the rational design and synthesis of tailored nanostructures. To date, direct observation and fundamental understanding are still lacking for the spatial interaction between particles and their structural evolution in the colloidal reaction.[1] Most of efforts in the mechanism study have focused on the morphological characterization of dry samples using transmission electronic microscopy (TEM).

The generally realized anisotropic growth is due to the significant difference in the surface free energies or reactivity of various crystallographic planes of particles.[3,6,7] Therefore, different surface ligands were used to selectively bind to the respective surface planes for controlling the growth rates of different surfaces for the formation of nanorods in colloidal solution. Organic−inorganic interface or difference in the surface energy plays a critical role in manipulating the shape or morphology. In recent years, greater insight into the formation mechanism of anisotropic growth, named oriented aggregation or attachment mechanism, was reported.[8−19] The oriented attachment is a remarkable reaction mechanism, but its details remain unclear.[6,18] In recent years, the study of growth mechanism, including oriented attachment, has shown great potential in controlling and designing materials of various nanostructures. Many researchers experimentally and theoretically reviewed the growth mechanism. Most of them observed the morphologies using TEM combined with correlative techniques such as X-ray diffraction (XRD), ultraviolet (UV)−visible spectroscopy and X-ray photoelectron spectroscopy. For example, Boneschanscher et al.[20] showed how the interfacial self-assembly and oriented attachment of nanocrystals results in 2D metal chalcogenide semiconductors with a honeycomb superlattice. Luo et al.[21] developed a new and convenient preparation method for TiO_2 nanocrystals and obtained one-dimensional (1D), two-dimensional (2D), and three-dimensional (3D) architectures by the self-assembly of TiO_2 nanoparticles, and an oriented attachment mechanism was found to drive the tiny particles into 1D nanochains. In addition, several efforts are centered on the oriented attach-

Received: July 8, 2014
Revised: October 2, 2014
Published: October 2, 2014

dx.doi.org/10.1021/jp506780h | J. Phys. Chem. C 2014, 118, 26332−26340

ment of TiO_2 nanocrystallities to the hierarchical mesocrystals,[22] branched nanorods,[22] highly branched nanowire,[23] and nanosheet.[24] Lv et al.[25] provide an overview of the recent theoretical advances in oriented attachment kinetics combined with experimental evidence. However, the small-angle X-ray scattering (SAXS) characterization of the anisotropic growth of shaped nanoparticles in solution is still lacking. In our work, we employed the first combination of SAXS, TEM, and XRD to study the time-dependent behaviors of the TiO_2 nanorod formation in solution at different temperatures. Our research directly probes the reaction solution of nanoparticles by SAXS and deduces nanoparticle behaviors qualitatively and quantitatively at different temperatures for different reaction times.

Small-angle X-ray scattering technique is a powerful tool for accurately investigating the shape and size of a large number of nanoparticles in a bulk sample.[26] Recently, the SAXS technique was successfully used to probe the nucleation and growth of spherical nanoparticles that were self-assembled in the solutions. The SAXS results complementarily revealed insights into the reaction kinetics and mechanism as compared to those established by the microscopic tools.[27−32]

TiO_2 nanorods[3,33] were extensively investigated because of wide technological interests, such as solar energy conversion,[34−37] photocatalysis,[38] nanofabrication,[39] and sensors.[40] Although numerous chemical routes have been developed to synthesize crystalline TiO_2, the one-step and large-scale synthesis for highly crystallized anatase TiO_2 particles with controlled size and shape is still an open challenge. Cozzoli's group[3] developed a novel synthetic approach for controlling the anisotropic growth of anatase TiO_2 nanorods at low temperatures (80−100 °C) with oleic acid as chelating ligand or surfactant. In this approach, the titanium precursor was chemically modified by oleic acid followed by hydrolysis and condensation reactions in the presence of water. The shape of nanoparticles is controlled by the amount of water and reaction time. Formation of nanorods can be induced by fast hydrolysis of the modified precursor, whereas nearly spherical particles are obtained by slow hydrolysis. On the other hand, Zhang et al.[7] employed a high-temperature nonhydrolytic approach to manipulate the shape and size of anatase TiO_2 nanoparticles. They employed a similar approach; the titanium precursor was modified by long-chain oleylamine (OA) first, followed by high-temperature aminolysis (260 °C). Anatase TiO_2 nanorods were formed at low OA concentration, whereas spherical TiO_2 nanoparticles were obtained with an increased OA concentration. Similar reaction systems, such as Fe_2O_3, $MnFe_2O_4$, ZrO_2, $CoFe_2O_4$, ZnO, and other metal oxide nanoparticles, were prepared with fatty acid as stabilization and coordination reagent and primary amine as activation reagent.[7] The nanoscale characterization for mechanistic study was mainly based on the TEM observations with inherent limitations, including sample preparation, sampling, statistical error, local variation, etc.

In the present study, we adopted the low-temperature hydrolysis method[3] as a case study to prepare organic-capped anatase TiO_2 nanorods. The morphological studies reported by other preparation methods are also discussed for a comprehensive comparison. This work employed the combination of SAXS, TEM, and XRD to study the time-dependent behaviors of the TiO_2 nanorod formation in solution at different temperatures. The direct probing of the reaction solution of nanoparticles by SAXS allowed deducing nanoparticle behavior both qualitatively and quantitatively at different temperatures for different reaction times. The results providee in-depth understanding of the formation mechanism, including the structural evolution, interparticle interaction, and spatial orientation, of nanoparticles during the nucleation, growth, and oriented attachment (from nanodots to nanorods) steps. The reaction mechanism is proposed to begin with primary particles which are quickly aggregated into quasi-spherical nanoparticles as a hydroxyl-terminated monomer, followed by oriented attachment, and then through step polymerization into nanorods.[41] The present study demonstrates a critical phenomenon spatially driving the development of oriented attachment, which is the rate-determining step of the reaction. A natural 3D template, governed by the balance of interaction forces among different surface ligands and solvent molecules, allows the alignment of spherical nanodots (as monomers) into the ordering structure. The template facilitates the simultaneous step polymerization into the rod shape. The spatial distributions of nanorods and nanodot monomers coexist and interact with each other in the colloidal solution during the oriented aggregation process. This SAXS analysis points out for the first time that the presence of a natural template in colloidal solution plays an important role and acts as a driving force for the formation of nanorods. The multistep mechanism of nucleation and isotropic and anisotropic growth proposed herein can provide insight into the mechanism of oriented aggregation and attachment. This SAXS study also provides the relevant knowledge for the further aggregation of nanorods into nanowires or 3D network structures in solution.

EXPERIMENTAL SECTION

Titanium tetraisopropoxide ($Ti(OPr)_4$ or TTIP) as precursor was chemically modified by oleic acid into titanium oxocarboxylalkoxide $(C_{17}H_{33}COO)_xTi(OPr)_{4-x}$. Anatase TiO_2 nanorods were prepared using the fast hydrolysis of modified precursor in the oleic acid solution at 80−100 °C.[3] Oleic acid (120 g) was stirred vigorously at 120 °C for 1 h in a three-neck flask under Ar flow then cooled to 90 °C and maintained at this temperature. Titanium isopropoxide (17 mmol) was then added to the flask. After the mixture was stirred for 5 min, trimethylamine-*N*-oxide dihydrate (34 mmol) in 17 mL of water was rapidly injected. Trimethylamine-*N*-oxide dihydrate was used as a catalyst for polycondensation. This reaction was maintained at 100 °C and was continued for 9 h to ensure complete hydrolysis and crystallization. Then, the TiO_2 nanorod product was obtained in the oleic acid solutions. The nanorods were washed and precipitated by ethanol repeatedly to remove any residual surfactant. Finally, the TiO_2 nanorods were collected by centrifugation and then redispersed in chloroform or toluene. The powder XRD pattern was obtained using a Bruker D8 diffractometer which was used to confirm the ordered crystalline structure of anatase TiO_2 particles. A transmission electron microscope (JEOL JEM-1230) was employed to observe the morphology of TiO_2 particles. The samples for the XRD and TEM were extracted from the same reaction bath at different times after injection.

The SAXS experiments for the oleic acid and toluene solutions at 80 and 100 °C were performed using a Bruker NANOSTAR SAXS in-house instrument. Incident X-rays were generated using a rotating-copper target, and the scattered intensity was collected using a 2D multiwire channel detector. The details of the in-house SAXS experiment and instrumental configuration were described elsewhere.[42,43] The solution samples for SAXS measurements were sealed in cells with a

dx.doi.org/10.1021/jp506780h | J. Phys. Chem. C 2014, 118, 26332−26340

mica window. The SAXS intensity profiles were measured as a function of scattering vector Q ($= 4\pi/\lambda \sin(\theta/2)$; θ is the SAXS scattering angle, and λ is the incident radiation wavelength) using the standard data reduction procedures (e.g., background subtraction, angular averaging).[44] The typically obtained SAXS intensity profiles covered the Q range 0.01−0.3 Å^{-1}.

RESULTS AND DISCUSSION

Ordered Arrangement between Particles during Reaction in Solution. Time-dependent SAXS intensity profiles of the solutions (containing the oleic acid solvent, modified titanium precursor, water, etc.) hydrolyzed at 100 °C are shown in Figure 1. The SAXS profile at t = 0 min is from

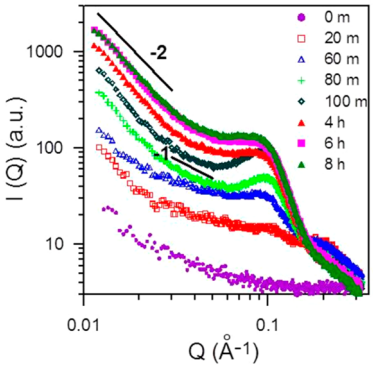

Figure 1. SAXS profiles for the oleic acid solutions extracted at different reaction times after the injection of water to induce the hydrolysis of modified precursor at 100 °C.

the scattering of small amount of agglomeration of TTIP−oleic acid complex (i.e., modified precursor) in the oleic acid solution before the addition of water.[3] For the SAXS profiles at t = 20 min to 8 h, the SAXS intensities in the low-Q region (0.01−0.05 Å^{-1}) demonstrate the two power-law scatterings and large increase compared to that at t = 0 min. The exponents of power-law scatterings are −2 and −1, respectively. Additionally, there is a significant structure factor peak due to the interaction between particles appearing in the mediate- and high-Q regions (0.05−0.2 Å^{-1}). The variation of SAXS profile shape with reaction time signifies the process of initial nucleation, anisotropic growth of Oleic acid-capped TiO_2 particles, spatial interaction of nanoparticles, and spatial network of nanorods in the solution. The time-dependent XRD patterns (Supporting Information; Figure S1) corresponding to this process show the temporal evolution of crystalline structure from partially crystallized phase at early stage to highly crystallized anatase phase. The XRD patterns are consistent with those reported by Cozzoli et al. using the same synthetic method.[3]

SAXS Analysis for Coexistence of Nanorods and Nanodots in Solution. It is not appropriate to directly analyze the complex SAXS profiles with structure factor peak (Figure 1) without any information on particle size and shape. To eliminate the effect of structure factor peak resulting from the ordering or interaction between particles in solution, we extracted oleic acid-capped TiO_2 nanoparticles from the above oleic acid solutions by filtering and washing processes. The oleic acid-capped TiO_2 nanoparticles were then well-dispersed in toluene. Figure 2 shows the SAXS profiles for these oleic acid-capped TiO_2 nanoparticles corresponding to different reaction times, which were dispersed in toluene. The disappearance of both the structure factor and low-Q scattering

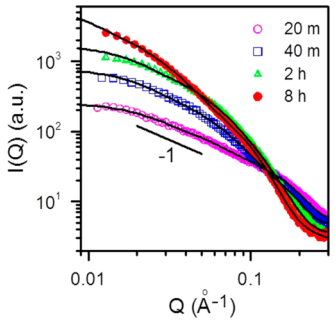

Figure 2. SAXS profiles for the toluene solutions containing the well-dispersed oleic acid-capped TiO_2 nanoparticles grown at 100 °C with different reaction times. The solid lines represent the SAXS intensities calculated by model fitting.

power ($\sim Q^{-2}$), describing the interparticle effect and spatial distribution of particles, indicates that oleic acid-capped TiO_2 nanoparticles are well-dispersed. The SAXS profiles (Figure 2) demonstrate the characteristics of form-factor of rod-like particles (i.e., the power-law scattering ($\sim Q^{-1}$) in the middle Q range).[26,45] Note that these SAXS profiles cannot be fitted with a simple form factor (either sphere or cylinder). They can be well fitted only by the model combining the form factors of polydispersed spheres and nanorods with polydispersed radii, as shown in Figure 2. The SAXS intensity, $I(Q)$, can be modeled by

$$I(Q) = \frac{f_c}{V_{poly}} \int_0^x f(r) \int_0^{\pi/2} F_c^2(Q, r, \alpha) \sin\alpha \, d\alpha \, dr + \frac{f_s}{V_{avg}} \Delta\rho^2 \int_0^\infty f(R) R^6 F_s^2(Q, R) \, dR + b \quad (1)$$

$$F_c(Q, r, \alpha) = 2(\pi r^2 L)\Delta\rho_c j_0\left(\frac{1}{2} QL \cos\alpha\right) \frac{J_1(Qr \sin\alpha)}{Qr \sin\alpha} \quad (2)$$

The first term on the right-hand side of eq 1 represents the SAXS intensity profile caused by cylinders with polydispersed radii normalized by the Schulz distribution, $f(r)$. The width of the radius distribution is defined by the polydispersity parameter, z. The volume fraction, length, and mean radius of cylinders are f_c, L, and $\bar{r}$, respectively. $F_c(Q,r,\alpha)$ is the scattering amplitude function for a cylinder with an oriented angle α relative to scattering vector.[26,44,45] $J_1(x)$ is the first Bessel function. The integration over all orientations α in eq 1 is calculated for the size-averaged form factor. The integration has been normalized by the second moment of the radius distribution. V_{poly} is the normalized volume of polydispersed cylinders using the second moment. The second term on the right-hand side of eq 1 represents the intensity resulting from polydispersed spheres having a Schulz size distribution of radius, $f(R)$, with a mean radius $\bar{R}$. $F_s(Q,R)$ is the scattering amplitude function for a sphere with radius R.[26,42,44] f_s and V_{avg} are the volume fraction and normalized volume of spheres, respectively. $\Delta\rho_c$ and $\Delta\rho$ are the scattering length density contrast for the cylinder and sphere, respectively. The constant b is the incoherent background. Two scattering contrast values fixed in the fitting calculation are very difficult to estimate accurately, so the relative volume fractions are determined in this work.

dx.doi.org/10.1021/jp506780h | J. Phys. Chem. C 2014, 118, 26332−26340

Temporal Behavior and Structural Evolution Determined by Quantitative SAXS Analysis and TEM Observation. The structural parameters obtained in the model fitting[44] of eq 1 are listed in Table 1. The mean sizes

Table 1. Structural Parameters of Polydispersed Spheres and Cylinders with Polydispersed Radii Obtained at Different Reaction Times and Temperatures

temp (°C)	time	f^a	$\bar{r}^a$ (nm)	L^a (nm)	z^a	$\bar{R}^b$ (nm)	z^b	f^b
100	20 m	0.21	1.7	23.4	0.40	1.4	0.05	0.50
	40 m	0.80	1.7	18.0	0.35	1.4	0.06	0.35
	2 h	0.82	1.9	18.9	0.31	1.6	0.13	0.32
	8 h	0.93	2.0	25.3	0.65	1.8	0.25	0.45
80	0 and 10 m					1.0		0.20
	20 and 40 m					1.0		0.50
	2 h	0.05	1.9	21.9	0.60	1.2	0.10	0.51
	4 h	0.67	1.8	26.0	0.60	1.5	0.16	0.41
	8 h	0.69	1.8	27.0	0.75	1.7	0.20	0.43
	10 h	0.64	1.8	28.0	0.80	1.7	0.20	0.42

[a]For the cylindrical particles. [b]For the spherical particles. z is the polydispersity. f is the relative volume fraction. R and r represent the radius. L is the rod length.

of the coexisting nanorods and spherical particles (Table 1) are consistent with our TEM observations, selectively shown in Figure 3. The TEM samples of the corresponding oleic acid solutions were prepared to analyze the diameter and length distributions (histograms) of nanorods and spherical particles as shown in the Supporting Information (Figure S2). Basically, the size and polydispersity of both kinds of particles determined by SAXS are relatively consistent with the supplementary TEM results. On the other hand, the mean diameter (~4 nm) and length (~27 nm) of TiO_2 nanorods determined by the SAXS analysis are approximately close to the size ranges reported by other groups.[3,17] However, the coexistence of spherical particles was not reported in their study. In fact, these spherical TiO_2 particles can be easily removed in the centrifugation and repeated washing processes during the synthetic procedure. Our analysis model of SAXS ignored the polydispersity in the length distribution of nanorods because the lowest Q value attainable (~0.12 $Å^{-1}$) is limited. In contrast, the SAXS characterization of diameter of nanorods is reliable. In a separate high-intensity synchrotron SAXS experiment extending the lowest Q value to ~0.065 $Å^{-1}$, we still obtain similar analysis results (Supporting Information; Figure S3).

Background of Mechanistic Understanding. The interpretation on the formation of the oleic acid-capped anatase TiO_2 nanorods, proposed in other studies using the hydrolytic[3] and nonhydrolytic[7] approaches, is based on the difference in surface energies (different ligands or functional groups selectively binding on the respective crystallographic surfaces). This would cause the surface-dependent growth rates. On the basis of this driving force, the particle shape (aspect ratio) or growth in length is time-dependent. However, the growth behavior of the TiO_2 nanorods revealed by our SAXS analysis (Table 1) is relatively insensitive to reaction time under our measurement conditions. This temporal variation cannot be substantially explained by the factor of surface energy only. On the other hand, for the case of surfactant-assisted elimination of

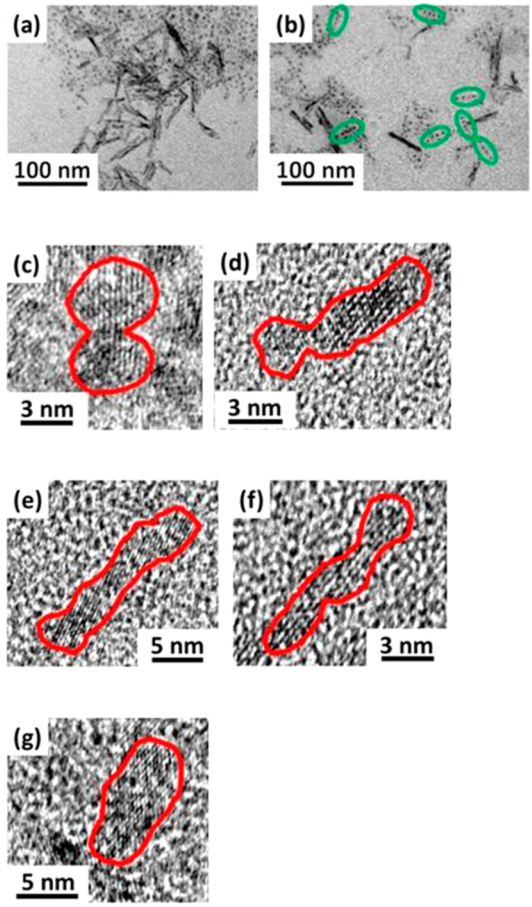

Figure 3. TEM images as examples taken from the oleic acid solutions at (a) 100 °C for 8 h and (b) 80 °C for 10 h. Green circles in (b) mark the pearl-chain-like structure. HRTEM images of some nanorods, (c)–(g), show the morphological evidence (outline is marked by red line; the inside displays clear crystalline structure) of oriented aggregation of primary nanodots.

high-energy facet, TEM observation of the morphology of TiO_2 nanoparticles shows the evolution from a bullet structure to a zigzag-shaped rod.[2] Our TEM observations are consistent with this report.

A review of the literature reveals several studies[8−10] that report that the oriented attachment mechanism occurs on the formation of some anisotropic TiO_2 crystals with complex shape and connectivity. This involves the calescence of faceted nanocrystals by reducing their total free surface energy.[6] The TEM observations of Oskam's group[46] demonstrated that the initial growth of spherical TiO_2 particles follows the Lifshitz−Slyozov−Wagner (LSW) model. After a prolonged time, the spherical particles would partially self-assemble in the epitaxial direction (considered to be oriented attachment). To our knowledge, few studies using comprehensive experimental results clearly address and confirm the formation mechanism of TiO_2 nanorods. The growth of both ZnS nanorods[12] and ZnO nanorods[11] is suggested to follow oriented attachment mechanism. However, their results are based on only TEM study using dry samples of particles. Note that our result demonstrates the coexistence of both spherical particles and nanorods, which is consistent with the report of Yu et al.[12] Moreover, our SAXS analysis would provide the insight into the mechanism involving the transformation from spheres to rods

dx.doi.org/10.1021/jp506780h | J. Phys. Chem. C 2014, 118, 26332−26340

via the oriented attachment, as shown in the Scheme 1 of ref 12. The TEM observation from ZnO nanodots to nanorods via oriented attachment (Figure 3a of ref 11) shows that quasi-spherical particles align in a pearl-chain-like structure, which is also observed in our TEM images (Figure 3b).

Kinetics and Formation of Nanorods via Formation, Alignment, and Attachment of Nanodots. To study the early stage of reaction in easily handled experiments, we lowered the reaction temperature to 80 °C to reduce the rate of reaction. Using the same synthetic procedure at 80 °C and then dispersing the particles in the toluene, the time-dependent SAXS profiles of the toluene solutions are shown in Figure 4. At

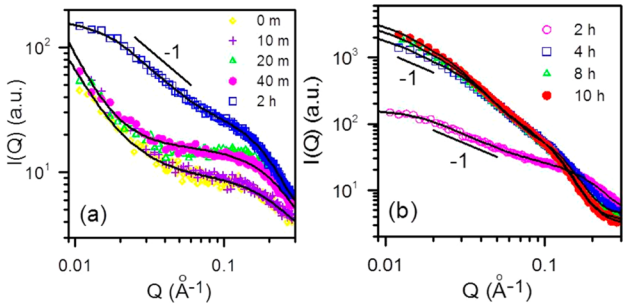

Figure 4. SAXS profiles for the toluene solutions corresponding to the similar syntheses at 80 °C for different reaction times. The solid lines represent the SAXS intensities calculated by model fitting.

t = 0–10 min, only spherical particles with a radius of ~1 nm formed through the burst nucleation and growth (the corresponding form factor profiles appeared in the high-Q region, 0.08–0.2 Å^{-1}). The low-Q region of scattering intensity can be attributed to the large agglomerates of precursor complex mentioned. When the time increased to 40 min, the volume fraction of spherical particles is increased but their sizes remain unchanged. Note that these quasi-spherical particles are considered to be monomers, which were formed in the early stage before the formation of nanorods. At t = 2 h, there is a dramatic increase in SAXS intensities (Figure 4). The SAXS profile shows the characteristics of nanorods with a power-law scattering (~Q^{-1}; 0.02–0.08 Å^{-1}). The previous SAXS profile in the high-Q region contributed by the spherical particles concurrently exists. The mean radius and length of nanorods determined by the model fitting (eq 1) are 1.9 and 22 nm, respectively (see Table 1). This result is close to that obtained at 100 °C for 2 h. When the time increased to 10 h, the mean radius of nanorods appears unchanged (~1.8 nm) but the rod length grows slightly (28 nm). The radius polydispersity of nanorods increases up to ~0.8 with increasing time. The length of nanorods can be speculated to have the similar polydispersity, although the growth of mean length is not obvious. It can be roughly concluded in this work that the temporal behavior of structural evolution of nanorods does not follow the conventional step polymerization: rod length grows gradually with time increase (i.e., chain length increases with time). From Table 1, the solutions at 80 °C (0–40 min) show the formation of only spherical particles with a fixed radius and increasing volume fraction. We define this (initial) stage as step I. The stage of oriented attachment of quasi-spherical particles into pearl-chain-like structure is step II. The subsequent step (termed step III) is that the nanorods with ~2 nm radius and ~22 nm length abruptly form (at t = 2 h), and then their growth (in radius, length, and volume fraction) is almost stable with increasing time (4–10 h). This is evidence of the mechanism of oriented attachment. The solutions at 100 °C show a similar process, while its first step (I) is relatively prompt.

Alignment and Attachment of Nanodots into Nanorods in a Spatially Lamellar Arrangement as Template. For the oleic acid solutions at 100 °C for 20 and 60 min (in Figure 1), the initially formed nanorods of 1.7 nm radius and 23 nm length (Table 1) coexisted with the spherical particles. The SAXS profiles in the high-Q region (0.06–0.3 Å^{-1}) demonstrate the first- and second-order structure peaks with the exact position ratio of 1:2, revealing the lamellae ordering (details are indicated by arrows in Figure 5a). According to the

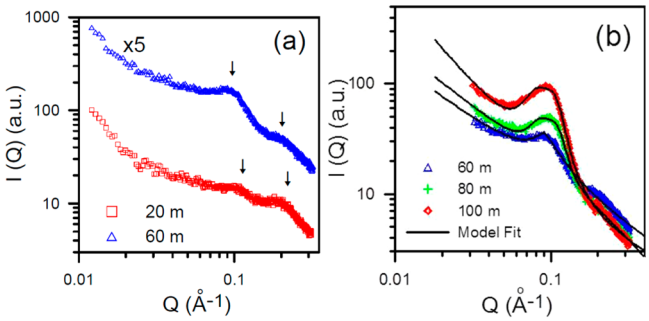

Figure 5. SAXS profiles selected from Figure 1. (a) The SAXS profiles, corresponding to t = 20 and 60 min, rescaled to show the first and secondary structure peaks of lamellae ordering. (b) The local structure peaks can be fitted well using the model (solid lines).

well-accepted rules, the lamellar structure describing the spatial interaction between particles can be evidenced by the structure peak of SAXS profiles when the ratio of peak position of the first-order and second-order peak is 1:2. In contrast, for the other ordered systems,[27] the position ratio is 1:$\sqrt{3}$ for the hexagonal-close-packed (HCP) structure. The position ratio is 1:$\sqrt{2}$ for the body-centered-cubic (BCC) structure. The lamellar layer comprises the spherical particles and nanorods. The corresponding SAXS profiles can be considered to be the product of the structural peaks and the form factor. It can be speculated that the several spherical particles aligning into a pearl-chain-like structure in the oleic acid solution coincides with the nanorods. The nanorods are concurrently formed with chain-like structure via proximity attachment between adjacent particles (discussed later). The appearance of the power law (~Q^{-1}) of Figure 1 shows that the nanorod is formed right after the formation of pure spherical particles (i.e., step I), signifying the oriented attachment mechanism. Moreover, in the early period of step II, the volume fraction of nanorods with stable size increases rapidly with the decrease in volume fraction of spherical particles (see Table 1; 20–40 m at 100 °C and 2–4 h at 80 °C). This situation suggests that nanorods are formed concurrently by the exhaustion of spherical particles, providing evidence of the oriented attachment mechanism. Both the chain structure and nanorod have similar diameters and are not distinguishable roughly in outline, contributing to the similar form factor in the SAXS intensity profiles. Herein, we define these spherical particles as the monomer particles which are present throughout the course of the reaction. In step II, the size of monomer particle may grow slightly (from 1.2 to 1.7 nm in radius for the case of 80 °C) but keep almost the same volume fraction (Table 1). This growth behavior can provide a reasonable explanation why the polydispersity of rod

dx.doi.org/10.1021/jp506780h | J. Phys. Chem. C 2014, 118, 26332–26340

radius increases during step II. The SAXS modeling approximated these monomer particles (namely, spherical-like, quasi-spherical, or even ellipsoid-like particles[17]) using the spherical geometry. This would lead to an error in the determination of radius. Because of the concurrent existence of polydispersity of monomer particles, the deviation in the size (due to aspect ratio) is difficult to be quantitatively justified. According to the mean radius of monomer particles, we can approximate that the major axis or average size of the ellipsoidal particles (in the real case[17]) is close to that of the nanorods (Figure 3c–g). Note that parts of the oriented attachment mechanism formed by such an alignment method[14,17] and attachment[16] between the adjacent monomer particles were evidenced or proposed by the recent studies.

Our TEM observations for a dry sample prepared from the oleic acid solution also shows the alignment of quasi-spherical monomer particles into a pearl-chain-like structure (Figure 3b). Moreover, our high-resolution TEM (HRTEM) images demonstrate morphological evidence of nanorod formation by the oriented attachment of monomer particles (Figure 3c–g). This HRTEM result is consistent with that of a recent HRTEM study on the direct observation of the oriented attachment in solution.[18] In step II, the quasi-spherical particles are formed by the partially anisotropic hydrolysis of spherical monomer particles of step I to grow in the preferential direction (see Supporting Information for details; Figure S4). Its global size is close to the diameter of the nanorod. The growth of the quasi-spherical particles and the subsequent alignment could occur simultaneously, as demonstrated by the temporal evolution of SAXS profiles. The lamellar structure (as demonstrated by the structure peak of SAXS profiles) comprising the quasi-spherical particles and nanorods may be speculatively regarded as the ordered arrays. The alignment into a chain (as a one-line array) is closely related to the ordered packing of the arrays. Then, finally in step III, nanorods are formed. The schematic representation of this possible scenario is shown in Figure 6.

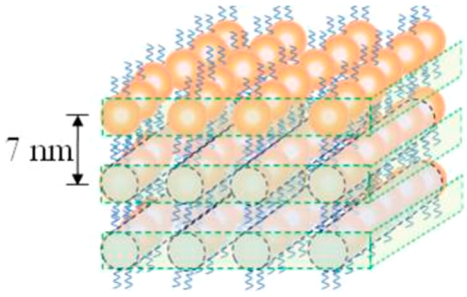

Figure 6. Schematic representation of quasi-spherical particles that are aligning into the chain structure and concurrently transforming to nanorods in the ordered lamellar structure as natural template in the solution.

Disruption of Lamellar Structure into a Simple Ordered System with Increasing Time. The SAXS model-fitting results (Table 1) show that the volume fraction of nanorods just formed increases with reaction time. When the reaction time is greater than 80 min, the lamellar structure (Figure 5a) is little disrupted to be a simple ordered system characterized by one structure peak (Figure 5b). The structure peak (at ~0.09 $Å^{-1}$) due to the interparticle effect shifts toward the low-Q region as the reaction time increases (Figure 1). This suggests the decrease of spacing of ordered arrays (i.e., more compact between nanorods). We attempt to determine structural information by empirically modeling this structural peak as follows:[44,47]

$$I(Q) = \frac{A}{Q^n} + \frac{C}{1 + (|Q - Q_0|\xi)^m} + B \quad (3)$$

where A and C are constants, n is the Porod exponent, m the Lorentzian exponent, and ξ the Lorentzian screening length. The first term is related to the power law's scattering contributed by the large-scale structure (discussed later). This models the intensity around the left-hand side of the structure peak. The second term (i.e., Lorentzian function) characterizes the interactions of particles.[44,47] The peak position at Q_0 is related to the d-spacing by $Q_0 = 2\pi/D$.

The spacing value D is a characteristic distance between the scattering inhomogeneities. The model fitting (eq 3) regarding to the structure peaks at different times is in good agreement with the measured intensities (Figure 5b). The best-fit values of Lorentzian screening length are ~4 nm for t = 60–100 min, which are close to the diameter of either the chain structure (quasi-spherical particles) or nanorods. This analysis result directly modeling the structure peak of SAXS profiles in oleic acid solutions is self-consistent with that using the combined form factors (eq 1) for the toluene solutions (particles dispersed in the solution). The d-spacing values of arrays according to the determined Q_0 values are ~7 nm. The d-spacing value corresponds to the distance between the centers of either nanorods or chain structures with a characteristic size, ξ ~ 4 nm (diameter).

Mechanistic Role of Lamellar Structure as Natural Template to Assist Oriented Attachment. This (ordered) lamellar structure formed in the oleic acid solution can be regarded as the result exerted by spatial interaction forces between particles and solvent molecules. In this structure, the formation (nucleation and growth) of monomer quasi-spherical particles, the alignment into the chain structure, and the formation of nanorods via proximity attachment (due to only the interfacial effect) are concurrently driven at the same positions or with the least displacement (Figure 6). This method of self-assembly (oriented attachment) is the most feasible path because it takes the smallest movement in short time (i.e., the least energy). This lamellar structure in the oleic acid solution seems to be constructed within a naturally nonvisible template. The hypothesis of a natural template proposed here can explain why the anisotropic growth (in the oriented attachment mechanism) is fast and easy. This natural template is probably formed by the balance of interaction forces among the anisotropic distribution of the various ligands on particles and solvent molecules.

It is well-known that the surfactant organization into micelles takes place when the critical micelle concentration (CMC) is reached. According to the systematic work of Cozzoli's group,[3] the CMC of TiO_2 synthesis for the self-assembly of molecules into initial particles is estimated to be in the molar ratio of 130:1 (oleic acid:TTIP) in oleic acid solution at 80 °C. From our TEM and SAXS results, we clearly observed the lamella structure, indicating the microreactor is in a lamella structure during the reaction.

Fractal Network of Nanorods Coexisting with the Development of a Natural Template. The SAXS intensity profiles (Figure 1) for the oleic acid solutions demonstrate two

dx.doi.org/10.1021/jp506780h | J. Phys. Chem. C 2014, 118, 26332–26340

patterns of power-law scatterings with the exponents of −2 and −1 (Q region, 0.01−0.05 Å^{-1}). This signifies the existence of fractal network structure (fractal dimension ∼2; with the open, self-similarity, and branched characteristics) aggregated by nanorods.[48−51] This large-scale fractal network structure coexists with the simple ordered (or lamellar) structure shown in the schematic representation of Figure 7. It can be

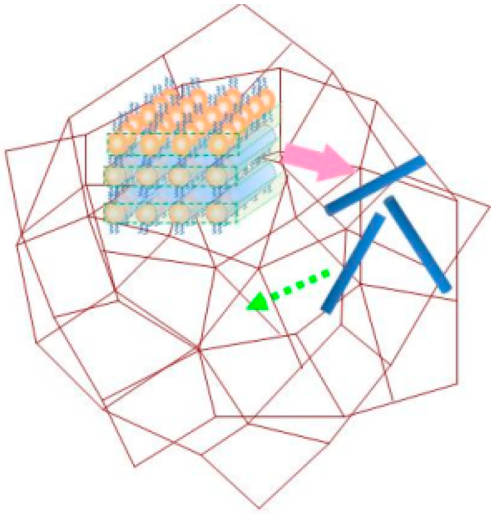

Figure 7. Schematic representation of the large-scale fractal network structure (brown) aggregated by nanorods (blue) in the oleic acid solutions. The nanorods are released from the lamellar structure concurrently existing with the fractal-like aggregation.

deduced that several nanorods formed by the oriented attachment. They were released from the lamellar template and then aggregate into a large fractal network structure. Our SAXS study cannot determine the real domains sizes of fractal network and lamellar structure because of the limitation of the Q-range. The progressive variation of SAXS intensities in the low-Q region (20 min to 4 h; Figure 1) demonstrates that the volume fraction of nanorods increases with reaction time (consistent with the result in Table 1). This is contributed mainly by the development of a lamellar structure (initially, 20−60 min) and then development of a fractal network (80 min to 4 h; with the disruption of lamellar template into a simple ordered system). However, when the reaction time was more than 4 h and up to 8 h, the temporal evolution of SAXS profiles saturates. This indicates that the structural evolution and formation of nanorods tend to stop after reaching the maximum values. This behavior is consistent with the observation of Cozzoli et al.[3] Because of the limitation of template size (Figure 6), large nanorods cannot be achieved. On the other hand, it is also very likely that the large fractal network aggregated by nanorods may assist the formation of a long chain by connecting the ends of nanorods.[52]

Details of Formation Mechanism. On the basis of the results of nanorod formation at 80 °C, the monomer particles grow from ∼1 nm (in step I) up to ∼1.7 nm during step II in spite of concurrent formation of nanorods. We propose that the spherical monomer particles (formed in step I) result from hydrolysis−condensations in all growth directions. The quasi-spherical particles are further formed by the partially anisotropic hydrolysis of primary particles growing in the preferential direction in step II. The hypothesized reaction mechanism of nucleation and growth of monomer particles is described in the Supporting Information (Figure S4). With the assistance of a natural template in the solutions, oriented attachment occurs to form pearl-chain-like structures (step II). Then the pearl-chain-like structure converts into a rod structure very rapidly as step III. Figure 8 illustrates a three-step

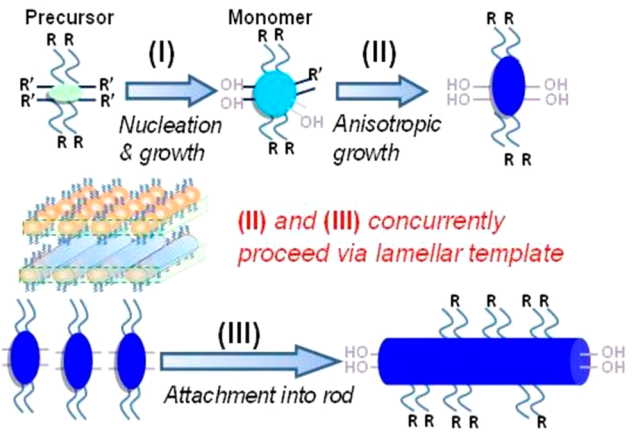

Figure 8. Schematic representation of formation of organic-capped TiO_2 nanorods via oriented attachment mechanism (R′ = −CH-$(CH_3)_2$; R = oleic acid ligand; OH = hydrolyzed functional group).

formation mechanism clearly. Herein, the dynamic removal and subsequent reconstruction of oleic acid molecules on the surface of the growing titania crystals are likely face-selective, which has been pointed out in the literature.[3] Although recent studies[14,16,17] reported similar finding about steps I and II, which are part of the mechanism, our study quantitatively provides all the details and the assistance of a natural template to grow into nanorods in step III. Separately, we have carried out the synthesis of nanorods at 98 °C at different times (2, 4, 6, 8, 9 h) batch-wise. The changes of rod dimension with time can be actually determined using XRD as shown in Table 2. We

Table 2. Size Variance of TiO_2 Nanorods Prepared at 98 °C with Different Reaction Times (As Determined by XRD Method)

reaction time (h)	width (nm)	length (nm)
2	3.64	21.0
4	3.72	23.8
6	4.04	23.8
8	4.10	26.4
9	4.62	29.7

did a linear fitting with the data. The result indicates that the reaction is a third-order reaction with a correlation coefficient of 0.89424 (Figure S5 of the Supporting Information). These kinetic results also support the three-step formation mechanism.

On the basis of the proposed mechanism, the spherical monomer particles frequently tuned by reaction conditions can affect the diameter of the rods and can be used to control the aspect ratio of the rods. The proposed mechanism may be applied to explain the detailed behavior of growth of diameter-tunable TiO_2 nanorods observed by Zhang et al.[7] Moreover, this working model of a nonvisible template in the solution assisting the alignment and formation of rods can be used to control the rod length and network structure of TiO_2

dx.doi.org/10.1021/jp506780h | J. Phys. Chem. C 2014, 118, 26332−26340

nanowires. It is also able to interpret the behavior of growth about the TiO_2 nanowires[13] and the recent research of oriented aggregation.[14] The present study can provide insight into the synthetic strategy of various nanoparticles and the control of nanostructure. The SAXS study regarding the solution state clearly addresses the details of formation mechanism of TiO_2 nanorods.

CONCLUSIONS

The first study on the oriented attachment mechanism using SAXS study for the formation of nanoparticles in solution is presented herein. The template (lamellar structure) formed by the natural balance of surface groups and solvent molecules assisted the oriented attachment in solution. The proposed mechanism provides insight into fundamental understanding of oriented attachment and its driving force, which is less investigated in this field. The SAXS analysis and TEM observation qualitatively and quantitatively provide sufficient interpretation on the mechanism, including the structural evolution, interparticle interaction, and spatial orientation of nanoparticles developed from nanodots to nanorods via the proposed multistep mechanism. The information is helpful for developing the strategy or synthesis parameters controlling the particle morphology and multilength-scale structures (from nanodot as basic unit to nanorod to wire network) by the oriented attachment. The oriented attachment mechanism revealed herein could provide more clues for solving the complex and unknown processes of various nanoparticle formations.

ASSOCIATED CONTENT

Supporting Information

XRD patterns, TEM images, TEM histogram, SAXS profiles, and curve fitting results. This material is available free of charge via the Internet at http://pubs.acs.org.

AUTHOR INFORMATION

Corresponding Authors

*E-mail: cstsao@iner.gov.tw.
*E-mail: suwf@ntu.edu.tw.

Notes

The authors declare no competing financial interest.

ACKNOWLEDGMENTS

We gratefully acknowledge the financial support from the National Science Council of Taiwan (NSC 101-2120-M-002-003, 101-3113-E-002-010, 102-2120-M-002-010) to carry out this research.

REFERENCES

(1) Maye, M. M.; Lim, I. S.; Luo, J.; Rab, Z.; Rabinovich, D.; Liu, T.; Zhong, C. J. Mediator-Template Assembly of Nanoparticles. *J. Am. Chem. Soc.* **2005**, *127*, 1519−1529.

(2) Jun, Y. W.; Casula, M. F.; Sim, J. H.; Kim, S. Y.; Cheon, J.; Alivisatos, A. P. Surfactant-Assisted Elimination of a High Energy Facet as a Means of Controlling the Shapes of TiO_2 Nanocrystals. *J. Am. Chem. Soc.* **2003**, *125*, 15981−15985.

(3) Cozzoli, P. D.; Kornowski, A.; Weller, H. Low-Temperature Synthesis of Soluable and Processable Organic-Capped Anatase TiO_2 Nanorods. *J. Am. Chem. Soc.* **2003**, *125*, 14539−14548.

(4) Peng, X.; Manna, L.; Yang, W.; Wickham, J.; Scher, E.; Kadavanich, A.; Alivisatos, A. P. Shape Control of CdSe Nanocrystals. *Nature (London, U.K.)* **2000**, *404*, 59−61.

(5) Peng, A.; Peng, X. G. Mechanism of the Shape Evolution of CdSe Nanocrystals. *J. Am. Chem. Soc.* **2001**, *123*, 1389−1395.

(6) Yin, Y.; Alivisatos, A. P. Colloidal Nanocrystal Synthesis and the Organic−Inorganic Interface. *Nature (London, U.K.)* **2005**, *437*, 664−670.

(7) Zhang, Z.; Zhong, X.; Liu, S.; Li, D.; Han, M. Aminolysis Route to Monodisperse Titania Nanorods with Tunable Aspect Ratio. *Angew. Chem., Int. Ed.* **2005**, *44*, 3466−3470.

(8) Penn, R. L.; Banfield, J. F. Imperfect Oriented Attachment: Dislocation Generation in Defect-Free Nanocrystals. *Science* **1998**, *281*, 969−971.

(9) Penn, R. L.; Banfield, J. F. Oriented Attachment and Growth, Twinning, Polytypism, and Formation of Metastable Phases: Insights from Nanocrystalline TiO_2. *Am. Mineral.* **1998**, *83*, 1077−1082.

(10) Alivisatos, A. P. Naturally Aligned Nanocrystals. *Science* **2000**, *289*, 736−737.

(11) Pacholski, C.; Kornowski, A.; Weller, H. Self-Assembly of ZnO: From Nanodots to Nanorods. *Angew. Chem., Int. Ed.* **2002**, *41*, 1188−1191.

(12) Yu, J. H.; Joo, J.; Park, H. M.; Baik, S.; Kim, Y. W.; Kim, S. C.; Hyeon, T. Synthesis of Quantum-Sized Cubic ZnS Nanorods by the Oriented Attachment Mechanism. *J. Am. Chem. Soc.* **2005**, *127*, 5662−5670.

(13) Adachi, M.; Murata, Y.; Takao, J.; Jiu, J.; Sakamoto, M.; Wang, F. Highly Efficient Dye-Sensitized Solar Cells with a Titania Thin-Film Electrode Composed of a Network Structure of Single-Crystal-like TiO_2 Nanowires Made by the "Oriented Attachment" Mechanism. *J. Am. Chem. Soc.* **2004**, *126*, 14943−14949.

(14) Yuwono, V. M.; Burrows, N. D.; Soltis, J. A.; Penn, R. L. Oriented Aggregation: Formation and Transformation of Mesocrystal Intermediates Revealed. *J. Am. Chem. Soc.* **2010**, *132*, 2163−2165.

(15) Cho, K. S.; Talapin, D. V.; Gaschler, W.; Murray, C. B. Designing PbSe Nanowires and Nanorings through Oriented Attachment of Nanoparticles. *J. Am. Chem. Soc.* **2005**, *127*, 7140−7147.

(16) Layek, A.; Mishra, G.; Sharma, A.; Spasova, M.; Dhar, S.; Chowdhury, A.; Bandyopadhyaya, R. A Generalized Three-Stage Mechanism of ZnO Nanoparticle Formation in Homogeneous Liquid Medium. *J. Phys. Chem. C* **2012**, *116*, 24757−24769.

(17) Menzel, R.; Cottam, B. F.; Ziemian, S.; Shaffer, M. S. P. Two-Stage, Non-Hydrolytic Synthesis for Improved Control of TiO_2 Nanorod Formation. *J. Mater. Chem.* **2012**, *22*, 12172−12178.

(18) Liao, H. G.; Cui, L.; Whitelam, S.; Zheng, H. Real-Time Imaging of Pt_3Fe Nanorod Growth in Solution. *Science* **2012**, *336*, 1011−1014.

(19) Penn, R. L. Kinetics of Oriented Aggregation. *J. Phys. Chem. B* **2004**, *108*, 12707−12712.

(20) Boneschanscher, M. P.; Evers, W. H.; Geuchies, J. J.; Altantzis, T.; Goris, B.; Rabouw, F. T.; Rossum, S. A. P. V.; Zant, H. S. J. V. D.; Siebbeles, L. D. A.; Tendeloo, G. V.; et al. Long-Range Orientation and Atomic Attachment of Nanocrystals in 2D Honeycomb Superlattices. *Science* **2014**, *344* (6191), 1377−1380.

(21) Luo, L.; Wang, P. P.; Jing, D.; Wang, X. Self-Assembly of TiO_2 Nanoparticles into Chains, Films and Honeycomb Networks. *CrystEngComm* **2014**, *16*, 1584−1591.

(22) Wang, H.; Liu, Y.; Liu, Z.; Xu, H.; Deng, Y.; Shen, H. Hierarchical Rutile TiO_2 Mesocrystals Assembled by Nanocrystals-Oriented Attachment Mechanism. *CrystEngComm* **2012**, *14*, 2278−2282.

(23) Li, D.; Soberanis, F.; Fu, J.; Hou, W.; Wu, J.; Kisailus, D. Growth Mechanism of Highly Branched Titanium Dioxide Nanowires via Oriented Attachment. *Cryst. Growth Des.* **2013**, *13*, 422−428.

(24) Li, F.; Xu, J.; Chen, L.; Ni, B.; Li, X.; Fu, Z.; Lu, Y. Nanosheet Array Assembled by TiO_2 Nanocrystallites with {116} Facets Parallel to the Nanosheet Surface. *J. Mater. Chem. A* **2013**, *1*, 225−228.

(25) Lv, W.; He, W.; Wang, X.; Niu, Y.; Cao, H.; Dickerson, J. H.; Wang, Z. Understanding the Oriented-Attachment Growth of Nanocrystals from an Energy Point of View: A Review. *Nanoscale* **2014**, *6*, 2531−2547.

(26) Guinier, A.; Fournet, G. *Small-Angle Scattering of X-Rays*; John Wiley and Sons: New York, 1955.

(27) Koizumi, S.; Hasegawa, H.; Hashimoto, T. Ordered Structure in Blends of Block Copolymers. 3. Self-Assembly in Blends of Sphere- or Cylinder-Forming Copolymers. *Macromolecules* **1994**, *27*, 4371−4381.
(28) Abecassis, B.; Testard, F.; Spalla, O.; Barboux, P. Probing in Situ the Nucleation and Growth of Gold Nanoparticles by Small-Angle X-ray Scattering. *Nano Lett.* **2007**, *7*, 1723−1727.
(29) Campi, G.; Mari, A.; Amenitsch, H.; Pifferi, A.; Cannas, C.; Suber, L. Monitoring Early Stages of Silver Particle Formation in a Polymer Solution by in Situ Time Resolved Small Angle X-Ray Scattering. *Nanoscale* **2010**, *2*, 2447−2455.
(30) Polte, J.; Ahner, T. T.; Delissen, F.; Sokolov, S.; Emmerling, F.; Thünemann, A. F.; Kraehnert, R. Mechanism of Gold Nanoparticle Formation in the Classical Citrate Synthesis Method Derived from Coupled in Situ XANES and SAXS Evaluation. *J. Am. Chem. Soc.* **2010**, *132*, 1296−1301.
(31) Polte, J.; Erler, R.; Thünemann, A. F.; Sokolov, S.; Ahner, T. T.; Rademann, K.; Emmerling, F.; Kraehnert, R. Nucleation and Growth of Gold Nanoparticles Studied via in Situ Small Angle X-ray Scattering at Millisecond Time Resolution. *ACS Nano* **2010**, *2*, 1076−1082.
(32) Schwahn, D.; Ma, Y.; Cölfen, H. Mesocrystal to Single Crystal Transformation of D,L-Alanine Evidenced by Small Angle Neutron Scattering. *J. Phys. Chem. C* **2007**, *111*, 3224−3227.
(33) Joo, J.; Kwon, S. G.; Yu, T.; Cho, M.; Lee, J.; Yoon, J.; Hyeon, T. Large-Scale Synthesis of TiO_2 Nanorods via Nonhydrolytic Sol−Gel Ester Elimination Reaction and Their Application to Photocatalytic Inactivation of *E. coli*. *J. Phys. Chem. B* **2005**, *109*, 15297−15302.
(34) Lin, J. F.; Wang, W. B.; Ho, C. C.; Jou, J. H.; Chen, Y. F.; Su, W. F. Enhancing P3HT/TiO_2 Hybrid Photovoltaic Performance by Incorporating High Surface Potential Polymeric Nanodot into Hole Transport Layer. *J. Phys. Chem. C* **2012**, *116*, 1955−1960.
(35) Tu, Y. C.; Lin, J. F.; Lin, W. C.; Liu, C. P.; Shyue, J. J.; Su, W. F. Improving Electron Mobility of TiO_2 Nanorods for Enhanced Efficiency of Polymer-Nanoparticle Solar Cell. *CrystEngComm* **2012**, *14*, 4772−4776.
(36) Zeng, T. W.; Lin, Y. Y.; Lo, H. H.; Chen, C. W.; Chen, C. H.; Liou, S. C.; Huang, H. Y.; Su, W. F. A Large Interconnecting Network within Hybrid MEH-PPV/TiO_2 Nanorod Photovoltaic Devices. *Nanotechnology* **2006**, *17*, 5387−5392.
(37) Wu, M. C.; Liao, H. C.; Cho, Y. C.; Chen, Y. F.; Su, W. F.; Kordas, K. Photo-Kelvin Probe Force Microscopy for Photocatalytic Performance Characterization of Single Filament of TiO_2 Nanofiber Photocatalysts. *J. Mater. Chem. A* **2013**, *1*, 5715−5720.
(38) Wu, M. C.; Hiltunen, J. T.; Sápi, A.; Avila, A.; Larsson, W.; Liao, H. C.; Huuhtanen, M.; Tóth, G.; Shchukarev, A.; Laufer, N.; et al. Nitrogen-Doped Anatase Nanofibers Decorated with Noble Metal Nanoparticles for Photocatalytic Production of Hydrogen. *ACS Nano* **2011**, *5*, 5025−5030.
(39) Wu, M. C.; Tóth, G.; Sápi, A.; Kónya, Z.; Kukovecz, Á.; Su, W. F.; Kordás, K. Synthesis and Photocatalytic Performance of Titanium Dioxide Nanofibers and the Fabrication of Flexible Composite Films from Nanofibers. *J. Nanosci. Nanotechnol.* **2010**, *12*, 1421−1424.
(40) Wang, C.; Wu, J. C.; Wang, P. F.; Ao, Y. H.; Hou, J.; Qian, J. Investigation on the Application of Titania Nanorod Arrays to the Determination of Chemical Oxygen Demand. *Anal. Chim. Acta* **2013**, *767*, 141−147.
(41) Liu, K.; Nie, Z.; Zhao, N.; Li, W.; Rubinstein, M.; Kumacheva, E. Step-Growth Polymerization of Inorganic Nanoparticles. *Science* **2010**, *329*, 197−200.
(42) Tsao, C. S.; Yu, M. S.; Chung, T. Y.; Wu, H. C.; Wang, C. Y.; Chang, K. S.; Chen, H. L. Characterization of Pore Structure in Metal-Organic Framework by Small-Angle X-ray Scattering. *J. Am. Chem. Soc.* **2007**, *129*, 15997−16004.
(43) Tsao, C. S.; Chen, C. Y.; Chung, T. Y.; Su, C. J.; Su, C. H.; Chen, H. L.; Jeng, U. S.; Yu, M. S.; Liao, P. Y.; Lin, K. F.; et al. Structural Analysis and Thermal Behavior of Pore Networks in High-Surface-Area Metal-Organic Framework. *J. Phys. Chem. C* **2010**, *114*, 7014−7020.
(44) Kline, S. R. Reduction and Analysis of SANS and USANS Data Using IGOR Pro. *J. Appl. Crystallogr.* **2006**, *39*, 895−900.
(45) Tsao, C. S.; Li, M.; Zhang, Y.; Leao, J. B.; Chiang, W. S.; Chung, T. Y.; Tzeng, Y. R.; Yu, M. S.; Chen, S. H. Probing the Room Temperature Spatial Distribution of Hydrogen in Nanoporous Carbon by Use of Small-Angle Neutron Scattering. *J. Phys. Chem. C* **2010**, *114*, 19895−19900.
(46) Oskam, G.; Nellore, A.; Penn, R. L.; Searson, P. C. The Growth Kinetics of TiO_2 Nanoparticles from Titanium(IV) Alkoxide at High Water/Titanium Ratio. *J. Phys. Chem. B* **2003**, *107*, 1734−1738.
(47) Hammouda, B.; Ho, D. L.; Kline, S. R. Insight into Clustering in Poly(ethylene oxide) Solutions. *Macromolecules* **2004**, *37*, 6932−6937.
(48) Bauer, B. J.; Hobbie, E. K.; Becker, M. L. Small-Angle Neutron Scattering from Labeled Single-Wall Carbon Nanotubes. *Macromolecules* **2006**, *39*, 2637−2642.
(49) Wang, H.; Zhou, W.; Ho, D. L.; Winery, K. I.; Fischer, J. E.; Glinka, C. J.; Hobbie, E. K. Dispersing Single-Walled Carbon Nanotubes with Surfactants: A Small Angle Neutron Scattering Study. *Nano Lett.* **2004**, *4*, 1789−1793.
(50) Zhou, W.; Islam, M. F.; Wang, H.; Ho, D. L.; Yodh, A. G.; Winery, K. I.; Fischer, J. E. Small Angle Neutron Scattering from Single-Wall Carbon Nanotube Suspensions: Evidence for Isolated Rigid Rods and Rod Networks. *Chem. Phys. Lett.* **2004**, *384*, 185−189.
(51) Li, Y. C.; Chen, K. B.; Chen, H. L.; Hsu, C. S.; Tsao, C. S.; Chen, J. H.; Chen, S. A. Fractal Aggregates of Conjugated Polymer in Solution State. *Langmuir* **2006**, *22*, 11009−11015.
(52) Rahman, M. H.; Chen, C. Y.; Liao, S. C.; Chen, H. L.; Tsao, C. S.; Chen, J. H.; Liao, J. L.; Ivanov, V. A.; Chen, S. A. Segmental Alignment in the Aggregate Domains of Poly(9,9-dioctylfluorene) in Semi-Dilute Solution. *Macromolecules* **2007**, *40*, 6572−6578.